An Optimal clutch-like control mechanism for Induction Motors Under Active Disturbance Rejection Control*

Juan Quecan-Herrera[1], Ruben Garrido[2] and Hebertt Sira-Ramírez[3]

***Abstract*— This paper presents the design of a clutch-like control mechanism for controlling an induction motor under the Active Disturbance Rejection Control (ADRC) strategy, assuming that the initial value of the angular position of the rotor is not equal to the initial value of the desired position trajectory. The clutch mechanism changes the amplitude of the control signals at the beginning of system operation to prevent excessive control signals. The mechanism is tuned using a Particle Swarm Optimization (PSO) algorithm. The reported results show that the clutch mechanism reduces the initial control voltage values compared with the case when the clutch mechanism is absent.**

***Index Terms*— Clutch-like control mechanism, ADRC, Optimization, Particle Swarm Optimization, Induction motor.**

I. INTRODUCTION

Induction motors have been considered for numerous applications such as transportation systems including automobiles and trains [1], [2]. They offer advantages such as low cost and compatibility with mature control techniques [3], [4]. In many applications, the main control scheme is based on the rotor-field-oriented control (FOC) approach [1], which introduces nonlinear system dynamics.

This electrical machine can be addressed using Active Disturbance Rejection Control (ADRC), a technique suitable for flat systems to cope with the effects of unmodeled dynamics, disturbances, and parametric uncertainties. The ADRC scheme was proposed by J.Q. Han [5] and has been used in numerous works, including [6], [7], [8] among others. However, ADRC has often been applied without considering the behavior of the control signal, in particular, when a large difference between the desired trajectory and the measured output, for example, under mismatched initial conditions between the system and the desired trajectory, which may produce large control signals potentially leading to actuator saturation and large oscillations.

To address this problem, a smooth and optimal transition in the control signal is required to reduce its magnitude during the transient stage. For the optimization stage, the PSO algorithm [9] is employed because it has been widely used for ADRC tuning and parameter identification [10], [11], [12], [13]. In this work, a time-varying inertia PSO variant [14] is adopted to improve the optimization performance.

Thus, the main contribution of this work is an optimal clutch-like mechanism based on a Bézier smooth signal for ADRC-based induction motor control, tuned using a PSO algorithm with time-varying inertia to reduce the initial control values under mismatched system initial conditions through a smooth transition.

This paper is organized as follows: Section II introduces the ADRC preliminaries. Section III explains the control design, the dynamics of the induction motor and its control scheme. Subsequently, the clutch mechanism is presented along with the optimization problem. Finally, the PSO algorithm is used for tuning the clutch mechanism. Section IV shows simulation results, and Section V concludes the paper.

II. PRELIMINARIES

Active Disturbance Rejection Control (ADRC)

ADRC is a robust nonlinear control strategy based on a model of a plant consisting of a perturbed chain of integrators. The disturbance includes nonlinear and unmodeled dynamics, internal and external disturbances, and uncertainties [5]. The scheme is based on an extended state observer (ESO), which estimates the disturbance and the system state, both used for designing a feedback control law that compensates the effect of disturbances thus enhancing robustness. Consider a nonlinear system:

$$\begin{aligned} \dot{x} &= f(x) + g(x)u, \quad x \in \mathbb{R}^n, \quad u \in \mathbb{R}. \\ y &= h(x), \quad y \in \mathbb{R}, \end{aligned} \tag{1}$$

where $f(\cdot)$ and $g(\cdot)$ denote vector fields, and y is the flat output that parametrizes x. Considering the relative degree of the flat-output dynamics n, it follows that $L_g L_f^k h(x) = 0$ for $k = 0, \ldots, n-2$, and $L_g L_f^{(n-1)} h(x) \neq 0$, where $L_f^{(n-1)} h(x)$ denotes the $(n-1)$th directional derivative of h with respect to the vector field f, and $L_g L_f^{(n-1)} h(x)$ denotes the directional derivative of $L_f^{(n-1)} h(x)$ with respect to the vector field g. Define:

$$\kappa(\underline{y}) := \kappa(y, \dot{y}, \ldots, y^{(n-1)}) = L_g L_f^{(n-1)} h(x), \tag{2}$$

then, the n-th derivative of the flat output can be expressed as:

$$\begin{aligned} y^{(n)} &= L_f^{(n)} h(x) + u\left(L_g L_f^{(n-1)} h(x)\right), \\ \xi(t) &:= L_f^{(n)} h(x), \\ y^{(n)} &= \kappa(y, \dot{y}, \ldots, y^{(n-1)})u + \xi(t) \\ y^{(n)} &= \kappa(\underline{y})u + \xi(t). \end{aligned} \tag{3}$$

*This work was supported by SECIHTI MEXICO through scholarship number 4045670, awarded to Juan Sebastian Quecan Herrera.

[1]Juan Quecan-Herrera is with Department of Automatic Control, CINVESTAV, Ciudad de México, México. juan.quecan@cinvestav.mx

[2] Ruben Garrido is with Department of Automatic Control, CINVESTAV, Ciudad de México, México. ruben.garrido@cinvestav.mx

[3]Hebertt Sira-Ramírez is with the Department of Electrical Engineering, CINVESTAV, Ciudad de México, México. hsira@cinvestav.mx

Define an auxiliary control input $v := \kappa(\underline{y})u$, its nominal value as the n-th derivative of the flat output reference, $v^*(t) := y^{*(n)}(t)$, and the errors $e_y = y - y^*(t)$ and $e_v = v - v^*(t)$, then, from (3):

$$e_y^{(n)} = e_v + \xi(t), \tag{4}$$

yielding the last equation of the Brunovsky canonical form for the tracking error dynamics. For the system described in (4), the ADRC controller expressed as a transfer function is designed as in [15] and is given by:

$$e_v = -\left(\frac{k_n s^n + k_{n-1}s^{n-1} + \ldots + k_1 s + k_0}{s(s^{n-1} + k_{2n-1}s^{n-2} + \ldots + k_{n+1})}\right) e_y. \tag{5}$$

For a pure integrator plant $G(s) = \frac{1}{s^n}$, the controller allows defining the closed-loop dynamics of the system because the dynamic of the system due to the characteristic polynomial of the closed-loop system is:

$$P_d(s) = s^{2n} + k_{2n-1}s^{2n-1} + \ldots + k_1 s + k_0, \tag{6}$$

where $P_d(s)$ is a product of two coprime polynomials of order n [15]:

$$\begin{aligned} P_d(s) &= P_o(s)P_c(s) \\ &= \left(s^n + \gamma_{n-1}s^{n-1} + \ldots + \gamma_1 s + \gamma_0\right) \times \\ &\quad \left(s^n + \lambda_{n-1}s^{n-1} + \ldots + \lambda_1 s + \lambda_0\right), \end{aligned} \tag{7}$$

$P_o(s)$ corresponds to an observer polynomial, and $P_c(s)$ corresponds to a controller polynomial. To ensure the equivalence between the ADRC scheme where a reduced order extended state observer (ROESO) is considered, and the controller described in (5), $P_c(s)$ and $P_o(s)$ have to be coprime and Hurwitz [15], [16]. This work considers first- and second-order systems. Based on the equivalence described in [17], the controller equivalent to an ADRC for a second-order system is:

$$\begin{aligned} e_v &= -\left(\frac{k_2 s^2 + k_1 s + k_0}{s(s + k_3)}\right) e_y \\ &= -\left(\frac{(\gamma_0 + \lambda_0 + \gamma_1\lambda_1)s^2 + (\gamma_0\lambda_1 + \gamma_1\lambda_0)s + \gamma_0\lambda_0}{s(s + \gamma_1 + \lambda_1)}\right) e_y, \end{aligned} \tag{8}$$

which corresponds to a PID controller with a dirty derivative term. For a first-order system, the equivalent controller takes the form:

$$e_v = -\left(\frac{\epsilon_1 s + \epsilon_0}{s}\right) e_y = -\left(\frac{(\gamma_0 + \lambda_0)s + \gamma_0\lambda_0}{s}\right) e_y, \tag{9}$$

which corresponds to a PI controller.

Characteristic polynomials: For a second-order system, it is possible to consider the following characteristic polynomial for the closed-loop system:

$$\begin{aligned} P_s(s) &= (s^2 + \gamma_1 s + \gamma_0)(s^2 + \lambda_1 s + \lambda_0) \\ &= s^4 + (\lambda_1 + \gamma_1)s^3 + (\gamma_0 + \lambda_0 + \gamma_1\lambda_1)s^2 \\ &\quad + (\gamma_0\lambda_1 + \gamma_1\lambda_0)s + \gamma_0\lambda_0. \end{aligned} \tag{10}$$

and for a first-order system, the following is considered:

$$\begin{aligned} P_f(s) &= (s + \lambda_0)(s + \gamma_0) \\ &= s^2 + (\lambda_0 + \gamma_0)s + \gamma_0\lambda_0. \end{aligned} \tag{11}$$

Both polynomials ($P_s(s)$ and $P_f(s)$) must be Hurwitz and appropriately chosen to ensure equivalence between classical controllers, such as PI and PID, and ADRC based on ROESO.

III. Design Methodology

In this section, the dynamics of the induction motor, the ADRC, and the proposed clutch mechanism are presented and analyzed. Next, a cost function that considers the initial control voltage values through the instantaneous power and the angular speed tracking error, based on angular position measurements, is presented. Finally, the PSO algorithm used for tuning the parameters of the clutch mechanism is described.

A. Induction motor dynamics

A three-phase induction motor under a two-frame transformation using the Clarke transformation (a/b frame) and under the FOC scheme (d/q frame) has the model described in [4]:

$$\frac{d\theta}{dt} = \omega, \tag{12}$$

$$\frac{d\omega}{dt} = \mu\psi_d i_q - \frac{1}{J}\tau_L - \frac{f}{J}\omega, \tag{13}$$

$$\frac{d\psi_d}{dt} = -\eta\psi_d + \eta M i_d, \tag{14}$$

$$\frac{di_d}{dt} = -\gamma i_d + \frac{\eta M}{\sigma L_R L_S}\psi_d + n_p\omega i_q + \eta M\frac{i_q^2}{\psi_d} + \frac{1}{\sigma L_s}u_d, \tag{15}$$

$$\frac{di_q}{dt} = -\gamma i_q - \frac{\eta M}{\sigma L_R L_S}\omega\psi_d - n_p\omega i_d - \eta M\frac{i_q i_d}{\psi_d} + \frac{1}{\sigma L_s}u_q, \tag{16}$$

$$\frac{d\rho}{dt} = n_p\omega + \eta M\frac{i_d}{\psi_d}, \tag{17}$$

where

$$\eta = \frac{R_R}{L_R}, \quad \beta = \frac{M}{\sigma L_R L_S}, \quad \gamma = \frac{M^2 R_R}{\sigma L_R^2 L_S} + \frac{R_S}{\sigma L_S},$$
$$\sigma = 1 - \frac{M^2}{L_R L_S}, \quad \mu = \frac{n_p M}{J L_R}.$$

In these equations, θ is the angular position of the rotor and ω is the angular speed. ψ_d is the flux in the d axis, while i_d and i_q are the currents in the d and q axes, respectively. The input voltages are u_d and u_q. The system parameters include the motor inertia J, the load torque τ_L, the number of pole pairs n_p, and the coefficient of viscous friction f, which is not considered in this work. The stator and rotor resistances are R_S and R_R. The inductances are L_S and L_R, while M is the mutual inductance.

B. Control scheme for the induction motor

This subsection describes the angular position control of the induction motor, which is achieved using three controllers: the i_d, i_q, and θ controllers, where a two-stage ADRC controller is used. The angular position reference is defined by a smooth curve that enables the system to reach a constant angular speed in steady state. The control scheme is based on [12], [18].

1) Flux estimator: To make the induction motor operate under the FOC scheme, the following flux estimator is first proposed, as described in [4], considering the dynamics described in (14) and (17):

$$\frac{d\hat{\rho}}{dt} = n_p\omega + \eta M\frac{i_d}{\hat{\psi}_d}, \quad \frac{d\hat{\psi}_d}{dt} = -\eta\hat{\psi}_d + \eta M i_d, \tag{18}$$

since the flux and its corresponding angle are not directly measurable. Using the flux estimator, the following ADRC scheme is proposed:

2) Current control: The first control scheme regulates the currents i_d and i_q modeled as a first-order system, where the voltages u_d and u_q act as the corresponding control signals. For the control design of i_d, based on the dynamics described in (15), it is necessary to define the errors $e_{id} := i_d - i_d^*$ and $e_{v-id} := \frac{1}{\sigma L_s}\bar{u}_d - \dot{i}_d^*$, where $\bar{u}_d$ is an intermediate control variable that will initially replace the actual control variable u_d. Then, using (15) and the previously defined errors:

$$\dot{e}_{id} = e_{v-id} + \xi_d(t), \tag{19}$$

where $\xi_d(t) = -\gamma i_d + \frac{\eta M}{\sigma L_R L_S}\psi_d + n_p\omega i_q + \eta M\frac{i_q^2}{\psi_d} + \bar{\phi}_d$, with $\bar{\phi}_d$ representing possible disturbances, uncertainties, and unmodeled or unknown dynamics. Therefore, the proposed intermediate controller is defined as:

$$\bar{u}_d(s) = -L_s\sigma\left(\frac{\epsilon_1 s + \epsilon_0}{s}\right)(i_d(s) - i_d^*(s)) + L_s\sigma s i_d^*(s), \tag{20}$$

where i_d^* is the reference value of i_d. Similarly, for i_q, the intermediate controller is given by:

$$\bar{u}_q(s) = -L_s\sigma\left(\frac{\epsilon_1 s + \epsilon_0}{s}\right)(i_q(s) - i_q^*(s)) + L_s\sigma s i_q^*(s), \tag{21}$$

where i_q^* is the reference for i_q and $\bar{u}_q$ is considered an intermediate control variable that will initially replace the actual control variable u_q. To reduce the complexity of the control scheme, the current derivative terms $L_s\sigma s i_q^*(s)$ and $L_s\sigma s i_d^*(s)$ in (20) and (21) can be considered as additional disturbances ξ_d and ξ_q to reduce the design complexity considering they are bound to maintain the stability described in Appendix A.

3) Angular position control: The second control scheme regulates the angular position. Considering the induction motor dynamics described in (12) and (13), an auxiliary control variable is introduced via i_q^*. It is necessary to define the errors $e_\theta := \theta - \theta^*$ and $e_{v-\theta} := \mu\psi_d\bar{i}_q^* - \ddot{\theta}^*$, where $\bar{i}_q^*$ represents an intermediate control or a partial reference value of i_q that will initially replace the actual auxiliary control variable i_q^*. As a result of (12), (13) and the previously defined errors:

$$\ddot{e}_\theta = e_{v-\theta} + \xi_\omega(t), \tag{22}$$

where $\xi_\omega(t) = -\frac{1}{J}\tau_L - \frac{f}{J}\omega + \bar{\phi}_\theta$, with $\bar{\phi}_\theta$ representing the associated disturbance and/or uncertainties. Therefore, the intermediate control related to i_q^* is given by:

$$\bar{i}_q^*(s) = -\frac{1}{\mu\psi_d}\left(\frac{k_2 s^2 + k_1 s + k_0}{s(s+k_3)}\right)(\theta(s) - \theta^*(s)) + \frac{1}{\mu\psi_d}s^2\theta^*(s). \tag{23}$$

The actual control and/or reference signals are constructed in the following subsection through the clutch mechanism, using the intermediate control variables $\bar{u}_d$, $\bar{u}_q$, and $\bar{i}_q^*$.

C. Clutch-like control mechanism

Using the intermediate control variables described in (20), (21) and (23), the following control signals are considered for the induction motor:

$$i_q^*(t) = \bar{i}_q^* F_s(t), \quad u_d(t) = \bar{u}_d F_s(t), \quad u_q(t) = \bar{u}_q F_s(t), \tag{24}$$

where i_q^*, u_d and u_q are the actual control signals for the induction motor and $F_s(t)$ is the clutch mechanism.

Clutch mechanism $F_s(t)$: The clutch mechanism $F_s(t)$ is a smooth function given by:

$$F_s(t) = \begin{cases} p_i, & t < t_1 \\ p_i + (1 - p_i)\left(3\tau^2 - 2\tau^3\right), & t_1 \le t \le t_2 \\ 1, & t > t_2, \end{cases} \tag{25}$$

where $\tau = \frac{t-t_1}{t_2-t_1}$, p_i is the initial percentage of the initial control signal, and t_1 and t_2 are the absolute times that allow a smooth transition. In this case, p_i, t_1 and t_2 are adjusted as a part of the optimization problem. Graphically, $F_s(t)$ is shown in Fig. 1.

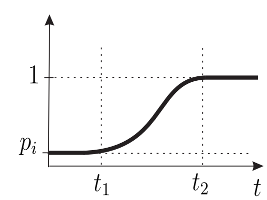

Fig. 1: Clutch-like control mechanism $F_s(t)$

D. Optimization problem

To address the issue arising from the mismatch between the rotor's initial angular position and the desired position trajectory, the following cost function is considered:

$$J = \int_{t_0}^{t_f}\Big(k_1\left|u_d(\tau)i_d(\tau) + u_q(\tau)i_q(\tau)\right|e^{-80\tau} + k_2\left|\omega(\tau) - \omega^*(\tau)\right|\Big)d\tau, \quad k_1, k_2 \in \mathbb{R}, \tag{26}$$

where t_0 and t_f are the initial and final operation times, respectively. The cost function aims to minimize the initial voltage values of the system regulating the current values through the instantaneous power in the d/q frame, while maintaining good performance in terms of the angular position tracking error, based on the derivative of the angular position reference: $\omega^* := \dot{\theta}^*$. Additionally, the constraints for the optimization problem are defined as follows:

$$0 \leq t_1 \leq 0.015, \quad 0.015 \leq t_2 \leq 0.3, \quad 0.001 \leq p_i \leq 0.15, \quad k_1 = 6, \quad k_2 = 10. \tag{27}$$

The initial value of p_i is constrained by the stability conditions in Appendix A, and t_1 and t_2 satisfying $t_1 < t_2$, allowing a fast transition. Therefore, the PSO algorithm is employed to solve the optimization problem. The value -80 in the exponential term prioritizes the initial instantaneous power, mainly during the first 30ms. The values of k_1 and k_2 are defined so that the different components of the composite cost function contribute adequately to the total cost, balancing voltage reduction and tracking performance.

Particle Swarm Optimization (PSO) Algorithm : For this optimization problem, the PSO algorithm is employed. The algorithm used is based on [19], [14], and is described as follows:

Algorithm 1: Basic Particle Swarm Optimization (PSO)

Data: Objective function J, bounds lb, ub, number of particles noP, max iterations $maxIter$
Result: Best solution $GBEST.X$

```
Initialize particles X_k ∈ [lb, ub], velocities V_k ;
Set PBEST_k.X ← X_k, PBEST_k.O ← J(X_k) ;
Set GBEST as the best among all PBEST_k ;
for t = 1 to maxIter do
    Update inertia weight w ;
    foreach particle k do
        Evaluate J(X_k) and update PBEST_k if needed ;
        Update GBEST if PBEST_k is better ;
        V_{k+1} ← wV_k + rand()(PBEST_k.X − X_k)c_1;
                 +rand()(GBEST.X − X_k)c_2 ;
        X_{k+1} ← X_k + V_{k+1} ;
```

For this work the following definition of w is used: $w = w_{max} - t\left(\frac{w_{max} - w_{min}}{maxIter}\right)$, where w_{max} and w_{min} are the maximum and minimum inertia values, respectively. This variation has been widely used, as described in [14]. Thus, the proposed control scheme is given by:

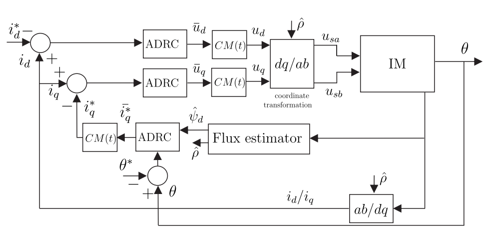

Fig. 2: Control scheme

Where the clutch scales the output of the ADRC controllers during the transient, generating the quadrature current reference and the effective a/b voltages while keeping the ADRC structure intact.

IV. Simulation Results

This section presents simulations using the PSO-based parameters obtained from the cost function J in (26) for different initial angular positions θ of the induction motor. The results show lower initial control voltages compared to the traditional ADRC.

A. System, algorithm and controller parameters

For the simulation results, and according to [18], the following parameters were considered for the induction motor previously described: $n_p = 1$, $J = 2 \times 10^{-3}$ [kg $\cdot$ m^2], $M = 0.2374$ [H], $L_R = 0.2505$ [H], $L_S = 0.2505$ [H], $R_S = 4.32$ [Ω], and $R_R = 2.8807$ [Ω]. Additionally, the following conditions were applied during the simulation tests $|i_q^*| \leq 6$, $\tau_L = 0.1(1-\cos(\pi t))$, $i_d^* = 1.5$ [A] and $f \approx 0$. The value of i_q^* is bounded to prevent the system from reaching large values or experiencing instability.

For the PSO in Algorithm 1, three variables are optimized within bounds [0, 0.015, 0.001]–[0.015, 0.3, 0.15], using 15 particles and 15 iterations. The inertia weights are $w_{\max} = 1$, $w_{\min} = 0.1$, and $c_1 = c_2 = 1.41$. The values of the PSO parameters are selected based on the convergence behavior of the algorithm [20]. Regarding the inertia weight, the initial value promotes exploration, while the final value favors convergence. For the controller design, the characteristic polynomials described in (10) and (11) must be coprime. Therefore, by using frequency methods [16], the magnitudes of the observer-related roots ($s^2 + \lambda_1 s + \lambda_0$ for second-order systems and $s + \lambda_0$ for first-order systems) must be greater than the magnitudes of the controller roots ($s^2 + \gamma_1 s + \gamma_0$ for second-order systems and $s + \gamma_0$ for first-order systems). Thus, the following values are proposed:

TABLE I: Parameters of ADRC controllers

System	λ_1	λ_0	γ_1	γ_0
Second-order	400	40000	40	400
First-order	–	1000	–	100

For the selection of controller parameters, the magnitude ratio between the controller roots and the observer roots is set to 1:10.

B. PSO Algorithm results

For this subsection, the induction motor previously described with an initial position of $\theta(0) = 15°$ was considered. The desired trajectory was defined by a Bézier polynomial with an initial value of $\theta^*(0) = 0$, resulting in a difference of $15°$. Using the PSO previously described under 15 different tests, the following statistics of the clutch mechanism described in (25) were obtained:

TABLE II: PSO Algorithm results

Variable	p_i	t_1	t_2	J
Mean	0.0364	0.0140	0.1158	11.4507
Worst case	0.0357	0.0109	0.1192	11.7053
Best case	0.0364	0.0150	0.1135	11.3555
Standard deviation	0.0033	0.0015	0.0045	0.1313

Table II shows similar results across the 15 experiments in terms of standard deviation and mean cost. In the simulations, the best clutch-based case is compared with the induction motor without the mechanism under mismatched initial rotor and reference positions.

C. Induction motor simulation results

Clutch-like control mechanism results: Considering the best values of the clutch mechanism tuned via PSO in Table II, the resulting control system behavior is presented as follows: Figure 3 shows the clutch mechanism results considering the initial condition of the PSO tuning ($\theta(0) - \theta^*(0) = 15°$) . Additionally, to compare the performance defined by J in (26), the clutch mechanism (CM) is evaluated against the system without it (NoCM) using three initial angle differences: $\theta(0) - \theta^*(0) = 15°$ (used in the optimization), $\theta(0) - \theta^*(0) = 10°$ and $\theta(0) - \theta^*(0) = 5°$. The comparison results are shown in Figures 4, 5, and 6.

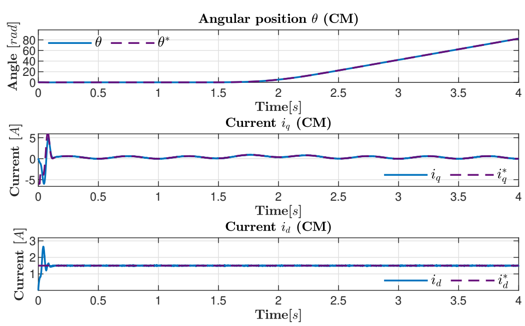

Fig. 3: Induction motor control response using a clutch-like control mechanism (CM)

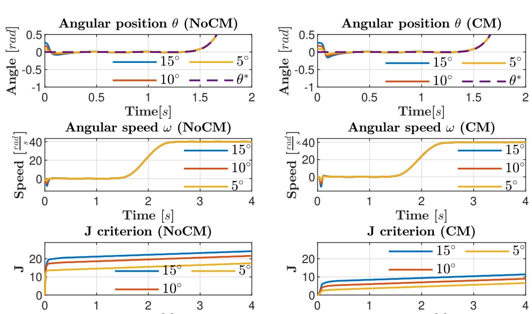

Fig. 4: Comparison results: Clutch-like control mechanism (CM) and traditional control scheme (NoCM)

Results in Figure 3 show that the system tracks the reference for d/q currents and angular position in steady state using $\theta(0) - \theta^*(0) = 15°$. Figure 4 indicates that the clutch mechanism improves performance according to the cost function in (26), while maintaining performance similar to that of the system without the mechanism in terms of tracking error. In Figure 5, when the mechanism is not used (NoCM), the peak voltage of v_{sa} (phase a in the a/b frame) reaches 180 V, approximately, while with the clutch mechanism (CM) it remains near 50V, mitigating saturation and physical issues. Figure 6 shows a higher ISE for CM due to reduced initial voltages, although both schemes achieve good tracking. Overall, the clutch-like control can replace the traditional ADRC, as it maintains similar responses while reducing initial control voltage.

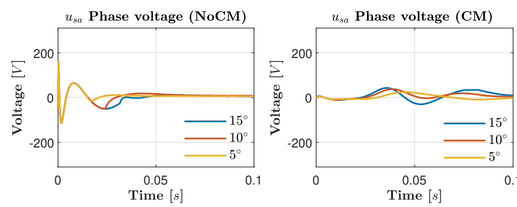

Fig. 5: Comparison results: Voltage u_{sa} using the proposed clutch control mechanism (CM) and control scheme without the clutch mechanism (NoCM)

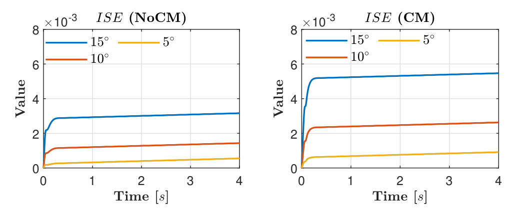

Fig. 6: Comparison results: ISE criterion using a clutch-like control mechanism (CM) and traditional control scheme (NoCM)

V. Conclusions

Issues arise in induction motor control with ADRC when the initial angular position is unknown. The mismatch between the desired trajectory and the actual position can produce high initial voltage demands, affecting both the controller and hardware. This paper shows that a clutch-like control mechanism tuned with the PSO algorithm reduces the initial voltage, improving saturation handling and respecting actuator limits. The approach provides an effective way to condition ADRC controllers regarding energy demands. Based on the simulation results, future work will address real-time implementation of the optimal clutch and sensitivity analysis of the optimization problem for reproducibility.

Appendix A

UUB Lyapunov Stability for a modified ADRC

This appendix analyzes the clutch mechanism in (25) for $0 < p_i < 1$, representing the worst-case ADRC scenario. First- and second-order systems are studied separately. Higher-order cases are outside the scope of this work but may be addressed through cascaded ADRC structures. Let X, E, and D denote the maximum positive values of the disturbance, disturbance estimation error, and x_2 estimation error, respectively, assuming observer stability [21].

First-Order System: For a first-order system, based on (4), using the clutch-like control mechanism p_i in the control law e_v: $\dot{e}_y = e_v + \xi, \quad e_v = p_i(-\gamma_0 e_y - \hat{\xi})$, defining $e_\xi := \xi - \hat{\xi}$, the closed loop dynamic is:

$$\dot{e}_y = -\gamma_0 p_i e_y + p_i e_\xi + (1 - p_i)\xi. \tag{28}$$

Assuming that e_ξ and ξ are bounded, with $e_\xi \leq |e_\xi| \leq E$ and $\xi \leq |\xi| \leq X$, with the following Lyapunov candidate function $V = \frac{1}{2}e_y^2$, then:

$$\dot{V} \leq |e_y|(-\gamma_0 p_i |e_y| + p_i E + (1 - p_i)X), \tag{29}$$

which yields the ultimate bound B:

$$B = \left\{ e_y : |e_y| \leq \frac{p_i E + (1-p_i)X}{p_i \gamma_0} \right\}. \tag{30}$$

For $p_i = 1$ (steady state condition), $B = \{e_y : |e_y| \leq \frac{E}{\gamma_0}\}$. Hence, UUB stability depends on a good estimation and the stability of the ROESO.

Second-Order System: For a second-order system, based on (4), using the the clutch-like control mechanism p_i in the control law e_v: $\ddot{e}_y = e_v + \xi$, $e_v = p_i(-\gamma_0 x_1 - \gamma_1 \hat{x}_2 - \hat{\xi})$, with $x_1 = e_y$, $x_2 = \dot{e}_y$, $e_2 = x_2 - \hat{x}_2$, and $e_\xi = \xi - \hat{\xi}$:

$$\dot{x}_2 = -\gamma_0 p_i x_1 - \gamma_1 p_i x_2 + \gamma_1 p_i e_2 + (1 - p_i)\xi + p_i e_\xi. \tag{31}$$

Assuming e_ξ, ξ and e_2 are bounded with $e_\xi \leq |e_\xi| \leq E$, $\xi \leq |\xi| \leq X$ and $e_2 \leq |e_2| \leq D$, with the following Lyapunov candidate function $V = \frac{1}{2}(x_1^2 + x_2^2)$, then:

$$\dot{V} \leq \|x\|\big((1 - \gamma_0 p_i - p_i \gamma_1)\|x\| + \gamma_1 p_i D + (1 - p_i)X + p_i E\big). \tag{32}$$

Thus, the ultimate bound B:

$$B = \left\{ x : ||x|| \leq \frac{\gamma_1 p_i D + (1-p_i)X + p_i E}{p_i(\gamma_0 + \gamma_1) - 1} \right\}. \tag{33}$$

Remark 1. *For second-order systems, to guarantee the well-defined bound B, the denominator $p_i(\gamma_0 + \gamma_1) - 1$ must be positive. Then, the value of p_i must satisfy $p_i > \frac{1}{\gamma_0 + \gamma_1} \approx 0.0023$ which motivates the lower bound in the optimization problem.*

With $p_i = 1$ (steady state condition) and a good estimation and the stability of the ROESO, the final bound becomes $B = \left\{ x : ||x|| \leq \frac{\gamma_1 D + E}{\gamma_0 + \gamma_1 - 1} \right\}, \quad \gamma_0 + \gamma_1 > 1.$

ACKNOWLEDGMENT

This work was supported by SECIHTI (Mexico) scholarship No. 4045670 and by CINVESTAV.

REFERENCES

[1] J. Rodriguez, C. Garcia, A. Mora, S. A. Davari, J. Rodas, D. F. Valencia, M. Elmorshedy, F. Wang, K. Zuo, L. Tarisciotti, F. Flores-Bahamonde, W. Xu, Z. Zhang, Y. Zhang, M. Norambuena, A. Emadi, T. Geyer, R. Kennel, T. Dragicevic, D. A. Khaburi, Z. Zhang, M. Abdelrahem, and N. Mijatovic, "Latest Advances of Model Predictive Control in Electrical Drives - Part II: Applications and Benchmarking With Classical Control Methods," *IEEE Transactions on Power Electronics*, vol. 37, no. 5, pp. 5047–5061, 2022.

[2] W. Lang, Y. Hu, C. Gong, X. Zhang, H. Xu, and J. Deng, "Artificial Intelligence-Based Technique for Fault Detection and Diagnosis of EV Motors: A Review," *IEEE Transactions on Transportation Electrification*, vol. 8, no. 1, pp. 384–406, 2022.

[3] Z. Wang, T. W. Ching, S. Huang, H. Wang, and T. Xu, "Challenges Faced by Electric Vehicle Motors and Their Solutions," *IEEE Access*, vol. 9, pp. 5228–5249, 2021.

[4] J. Chiasson, *Modeling and High-Performance Control of Electric Machines*. New York: John Wiley & Sons. Inc, 2005.

[5] J. Han, "From PID to active disturbance rejection control," *IEEE Transactions on Industrial Electronics*, vol. 56, no. 3, pp. 900–906, 2009.

[6] M. Tian, B. Wang, Y. Yu, Q. Dong, and D. Xu, "Discrete-Time Repetitive Control-Based ADRC for Current Loop Disturbances Suppression of PMSM Drives," *IEEE Transactions on Industrial Informatics*, vol. 18, no. 5, pp. 3138–3149, 2022.

[7] Y. Wang, S. Fang, and J. Hu, "Active Disturbance Rejection Control Based on Deep Reinforcement Learning of PMSM for More Electric Aircraft," *IEEE Transactions on Power Electronics*, vol. 38, no. 1, pp. 406–416, 2023.

[8] K. Lakomy, R. Madonski, B. Dai, J. Yang, P. Kicki, M. Ansari, and S. Li, "Active Disturbance Rejection Control Design with Suppression of Sensor Noise Effects in Application to DC-DC Buck Power Converter," *IEEE Transactions on Industrial Electronics*, vol. 69, no. 1, pp. 816–824, 2022.

[9] R. Eberhart and J. K. Sixth, "A new optimizer using particle swarm theory," *In: Proceedings of the IEEE Symposium on Micro Machine and Human Science, Nagoys, Japan*, pp. 39–43, 1997.

[10] D. Tristán-Rodríguez, O. Jiménez, R. Garrido, and E. Mezura-Montes, "Active disturbance rejection control: Tuning by pso considering stability conditions," in *2023 9th International Conference on Control, Decision and Information Technologies (CoDIT)*. IEEE, 2023, pp. 932–937.

[11] R. Cortez, R. Garrido, and E. Mezura-Montes, "Spectral richness pso algorithm for parameter identification of dynamical systems under non-ideal excitation conditions," *Applied Soft Computing*, vol. 128, p. 109490, 2022.

[12] Z. Yin, C. Du, J. Liu, X. Sun, and Y. Zhong, "Research on Autodisturbance-Rejection Control of Induction Motors Based on an Ant Colony Optimization Algorithm," *IEEE Transactions on Industrial Electronics*, vol. 65, no. 4, pp. 3077–3094, 2018.

[13] J. Quecan-Herrera, S. Rivera, J. Neira-garcía, and J. Cortés-romero, "Optimal active disturbance rejection control with applications in electric vehicles," *TELKOMNIKA*, vol. 23, no. 5, pp. 1427–1438, 2025.

[14] T. M. Shami, A. A. El-Saleh, M. Alswaitti, Q. Al-Tashi, M. A. Summakieh, and S. Mirjalili, "Particle Swarm Optimization: A Comprehensive Survey," *IEEE Access*, vol. 10, pp. 10 031–10 061, 2022.

[15] H. Sira-Ramírez, M. A. Aguilar-Orduña, and B. C. Gómez-León, "Active disturbance rejection control of nonlinear SISO Lagrangian systems via endogenous injections and exogenous feedback for trajectory tracking," *Control Theory and Technology*, vol. 19, no. 1, pp. 113–126, 2021.

[16] B. C. Gómez-León, M. A. Aguilar-Orduña, H. J. Sira-Ramírez, and R. A. Garrido-Moctezuma, "On the ADRC Control of Dynamically Feedback Linearizable Systems: A Cascade Buck-Buck DC-DC Converter Example," *American Control Conference*, pp. 2977–2982, 2024.

[17] H. Sira-Ramírez, "From flatness, GPI observers, GPI control and flat filters to observer-based ADRC," *Control Theory and Technology*, vol. 16, no. 4, pp. 249–260, 2018.

[18] H. Sira-Ramírez, J. Cortés-Romero, and A. Luviano-Juárez, "On the robust two-stage linear feedback control of the induction motor," *IECON Proceedings (Industrial Electronics Conference)*, pp. 1948–1953, 2011.

[19] S. Luke, *Essentials of Metaheuristics*, 2nd ed. Lulu, 2013, available for free at http://cs.gmu.edu/simsean/book/metaheuristics/.

[20] M. Clerc and J. Kennedy, "The particle swarm—explosion, stability, and convergence in a multidimensional complex space," *IEEE Transactions on Evolutionary Computation*, vol. 6, no. 1, pp. 58–73, 2002.

[21] H. Sira-Ramírez and E. W. Zurita-Bustamante, "On the equivalence between adrc and flat filter based controllers: A frequency domain approach," *Control Engineering Practice*, vol. 107, 2 2021.